Received: 11 April 2024 | Revised: 11 July 2024 | Accepted: 24 July 2024 | Published online: 29 July 2024

RESEARCH ARTICLE

Journal of Optics and Photonics Research
2024, Vol. 00(00) 1–9
DOI: 10.47852/bonviewJOPR42023085

BON VIEW PUBLISHING

Spectroscopy Study of Bismuth Lithium Strontium Borate Glasses Doped with Nd^{3+} Ions for 1.06 μm NIR-Emitting Glasses

R. Rajaramakrishna[1,2,*] and Evgenia Slyusareva[1]

[1]*Siberian Federal University, Russia*

[2]*Research Center for Optical Materials Science, ITMO University, Russia*

Abstract: $7Bi_2O_3$-$3.3Li_2O$-23SrO-(66.7-x) B_2O_3-xNd_2O_3 (where x = 0.0 (Nd0.0), 0.1 (Nd0.1), 0.3 (Nd0.3), 0.5 (Nd0.5) and 1 (Nd1.0) mol %) have been synthesized. Confirmation of unstructured nature of the glass was analyzed using XRD. Glass transition was obtained from differential scanning calorimeter for base glass and 1.0 mol% Nd_2O_3 content. UV-Vis-NIR studies were performed and studied Tauc plot with increase in Nd_2O_3concentration. Judd-Ofelt (JO) parameters Ω_λ ($\lambda = 2$, 4, and 6) were determined and have the following trend $\Omega_6 > \Omega_2 > \Omega_4$. All glass systems have been evaluated with amplification factor and found to be greater than unity. The present glasses doped with Nd^{3+} ion glass show best emission spectral intensity at $^4F_{3/2} \rightarrow {}^4I_{11/2}$ (1060 nm) with an excellent radiative transition probability. Using Judd-Ofelt intensity parameters and emission spectrum, the probabilities of radiative transition (A_R), lifetimes (τ_{rad}), full-width half maximum ($\Delta\lambda_{eff}$), and branching ratios (β_{rad} and β_{exp}) were estimated. Fluorescence transitions at $^4F_{3/2} \rightarrow {}^4I_{11/2}$. The 1.06 and 1.331 μm fluorescence bands are found to have the highest $\sigma_{emi}(\lambda)$ at 12.02×10^{-19} and 20.44×10^{-19} cm^2, respectively. The effective bandwidth, gain bandwidth, and optical gain suggest that 0.5 mol% of Nd_2O_3-doped glass may be a good option for creating O-band optical fiber amplifiers.

Keywords: neodymium, borate, Judd-Ofelt, NIR luminescence

1. Introduction

Strontium borate glasses show high merit toward thermal stability and wide optical transmission window; hence, it is ideal to make as glass host matrices [1–3]. SrO increases the glass-forming tendency by enhancing the randomness in the glass network and also established to increase in transition temperature [4]. The rare-earth ions' photoluminescence intensity can be enhanced quite a few times more than because of low phonon energies glass hosts usage [5, 6]. Oxide glasses, particularly Bi_2O_3 doped in borate glasses, are most appropriate hosts to obtain rare-earth ion luminescence efficiently [7, 8]. The addition of lithium to the B_2O_3 network causes the conversion of BO_3 to BO_4 groups up to certain alkali concentrations and exhibits excellent ultraviolet transmission [9]. UV–Vis-NIR absorption spectroscopy as a non-destructive [10] is an applicable technique for more than several decades to identify the signature electronic transition peaks of the elements in the materials and also the variations in their bond length [11]. The O states are mixed with the Ln ions having 5s, 5p, 4f, 6s, and 6p orbitals. O-2p and Ln 4f orbitals form the upper edge of the valence band, while Ln 5d and P-3s, 3p orbitals form the lower edge of the conduction band. Hence, these rare-earth ions contribute to electric-dipole sharp peaks with *f-f* transitions irrespective of its host [12]. Rare-earth ions doping in glasses show possess excellent physiochemical [5, 6], due to *f* orbit and significant luminescence properties. Also, RE^{3+} ions when added show energy transfer mechanism [13]. The radiative transition $^4F_{3/2} \rightarrow {}^4I_{11/2}$, for Nd^{3+} ions represents laser a transition at 1.06 μm in the NIR region [7]. Solid-state lasers, which operate at 1.06 μm wavelength, have attracted interest due to their potential uses in optoelectronics, medical diagnostics, photonic systems for optical storage with high density, and optical communication systems. One potential option for the optic material used in laser amplifiers is host matrix glass doped with Nd^{3+} ions. The energy level of the Nd^{3+} ion is ladder-like; for example, the $^4I_{11/2}$ level is positioned coarsely ~2000 cm^{-1} overhead the $^4I_{9/2}$ state. The original-band optical signal intensification at 1.3 μm and high-power lasers operating at 1.06 μm wavelength are known to be interesting regions which are found when Nd^{3+} ions are doped [14]. In this communication, the study is to focus on understanding the variation of Nd^{3+} ions and their effect in optical absorption properties, radiative and non-radiative transitions, and the role of Nd^{3+} affecting the bismuth lithium strontium borate structure. The chosen glass matrix is $7Bi_2O_3$-$3.3Li_2O$-23SrO-(66.7-*x*) B_2O_3-xNd_2O_3 where ($x = 0.1$, 0.3, 0.5, & 1.0) doped glasses are considered novel for the present study. The work also brings out the significance of 1.06 μm NIR emission by comparing with other reported literature with the present glass system.

2. Glass Synthesis and Instrumentation

Glasses doped with Nd_2O_3 were created using the appropriate concentrations of high-purity H_3BO_3, Li_2CO_3, SrO, and Bi_2O_3 with

*Corresponding author: R. Rajaramakrishna, Siberian Federal University and Research Center for Optical Materials Science, ITMO University, Russia. Email: rrajanavaneethakrishna@sfu-kras.ru

99.9% AR grade. The new stoichiometry ratio is $7Bi_2O_3$-$3.3Li_2O$-$23SrO$-$(66.7-x)$ B_2O_3-xNd_2O_3 where ($x = 0.1$, 0.3, 0.5, & 1.0) doped glasses was chosen. The precursor oxides were mixed thoroughly at standard temperature with 20 gm batch that were made and grinded into a fine powder transferred to porcelain crucible, which was placed in a muffle furnace to melt at 1100°C for 1 h where the heating rate was 10°C/min. The molten liquid melt poured in between the two brass discs and pressed homogeneously. To eliminate the thermal stress, the glasses were annealed for three hours at 200°C below the glass transition. The glasses were then polished using sand papers with various grit sizes from 320 to 2000 grade at various interval of time to get optical polish. X-ray diffractometer Philips X'Pert pro was used to obtain XRD, and Differential Scanning Calorimeter (DSC) was used to perform on powder $7Bi_2O_3$-$3.3Li_2O$-$23SrO$-$66.7B_2O_3$-xNd_2O_3 to measure transition temperature. Glass transition (Tg) was measured using a Mettler Toledo instrument at a heating rate of 10°C/min and a temperature range of 100°C to 550°C. Density measurements were employed by Archimedes principle, and refractive index was measured by Abbe refractometer. The UV-Vis-NIR spectra of polished samples were recorded with a UV-3600 Shimadzu spectrophotometer in the wavelength range 300–1000 nm. Using a Nd:YAG laser to excite the sample at 808 nm, photoluminescence spectra were obtained in the 800–1500 nm wavelength range.

3. Results and Discussion

3.1. Physical properties

The composition of the prepared glasses and their codes has been given in Table 1. Addition of Nd_2O_3 content impacts the refractive index due to heavy atomic mass Nd_2O_3 with replacement of low atomic mass of B_2O_3 restricts the movement of light. It was discovered that the density rose as Nd_2O_3 content from 3.567, 3.594, 3.621, 3.667, 3.713 g/cm^{-3} for 0.0Nd, 0.1Nd, 0.3Nd, 0.5Nd, and 1.0Nd glasses, respectively. Refractive index shows 1.628, 1.630, 1.657, 1.694, and 1.719 for 0.0Nd, 0.1Nd, 0.3Nd, 0.5Nd, and 1.0Nd glasses, respectively.

The density of the glass is influenced by the bond length between the atoms, which can be affected by the stretching force constants of the bonds that comprise the glass matrix. There are two reasons for the refractive index increase that has been observed: the exchange of lower molecular weight oxide B_2O_3 with Nd_2O_3 in the glass network, and the rigidity of the glasses, which will be covered in more detail in a later section of Judd-Ofelt theory. Changes in the glass network structure have been observed to impact polarizability, which is the reason for the observed increase in refractive index.

3.2. Structure and thermogram study

X-ray diffraction spectra of $7Bi_2O_3$-$3.3Li_2O$-$23SrO$-$(66.7-x)$ B_2O_3-xNd_2O_3 where ($x = 0.0$, 0.1, 0.5, & 1.0) doped glasses are shown in Figure 1. Figure 1 shows no sharp peaks suggesting that the prepared samples show amorphous in nature. Differential scanning calorimeter (DSC) thermogram of undoped and 1.0 mol% doped Nd_2O_3 samples obtained in the temperature ranges between 300°C–500°C. Figure 2 shows the glass transition temperature (T_g) for both undoped and 1.0 mol% Nd_2O_3 doped glasses. The value of T_g for 0.0Nd (Base glass) shows 428°C, and $7Bi_2O_3$-$3.3Li_2O$-$23SrO$-$66.7B_2O_3$-Nd_2O_3 glass shows 434°C. Increase in transition temperature was observed with increase in Nd_2O_3 content suggesting that Nd_2O_3 can enter the network forming sites by fragmenting B-O-B bonds/B-O-Bi bonds. The bond energies of B-O (809 kJ/mol) and Nd-O (703 kJ/mol) signify that lower bond energies of Nd-O are preferable to enter the network forming sites replacing B-O bonds; hence, the glass transition increases with addition of 1.0 mol% Nd_2O_3 content. Also, it is noted that the Nd^{3+} (0.983 Å) ions were replaced with Bi^{3+} (1.03 Å) ions, the overall polarizability relevant to the glasses' cations playing a part in influencing the rise in Tg and refractive index. But the higher densities of the glass system may also be responsible for the observed high Tg, which would explain the increased glass rigidity [15]. Due to such rigidity results in affecting their optical characteristics. To effectively withstand thermal damage, a glass must have a high T_g value. In the current study, the addition of Nd_2O_3 content indicates that they can withstand thermal damage when compared to undoped neodymium glass (base glass).

Figure 1
X-ray diffraction spectra of $7Bi_2O_3$-$3.3Li_2O$-$23SrO$-$(66.7-x)$ B_2O_3-xNd_2O_3 where ($x = 0.0$, 0.1, 0.5, & 1.0) doped glasses

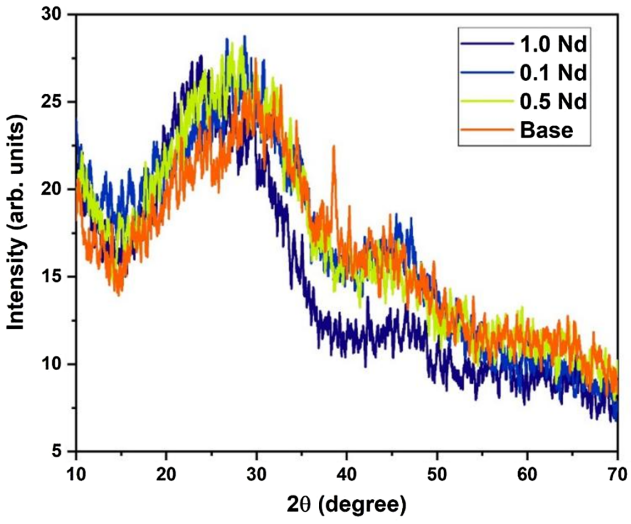

Table 1
Glass composition and codes

SI. NO.	Glass composition	Glass code	Density (g/cm^{-3})	Refractive index (n)
1	$7Bi_2O_3$-$3.3Li_2O$-$23SrO$-$66.7B_2O_3$-$0.0Nd_2O_3$	0.0Nd	3.567	1.628
2	$7Bi_2O_3$-$3.3Li_2O$-$23SrO$-$66.6B_2O_3$-$0.1Nd_2O_3$	0.1Nd	3.594	1.630
3	$7Bi_2O_3$-$3.3Li_2O$-$23SrO$-$66.4B_2O_3$-$0.3Nd_2O_3$	0.3Nd	3.621	1.657
4	$7Bi_2O_3$-$3.3Li_2O$-$23SrO$-$66.2B_2O_3$-$0.5Nd_2O_3$	0.5Nd	3.667	1.694
5	$7Bi_2O_3$-$3.3Li_2O$-$23SrO$-$65.7B_2O_3$-$1.0Nd_2O_3$	1.0Nd	3.713	1.719

Figure 2
Differential scanning calorimeter thermogram of $7Bi_2O_3$-$3.3Li_2O$-23SrO-(66.7-x) B_2O_3-xNd_2O_3 where (x = 0.0, & 1.0) doped glasses

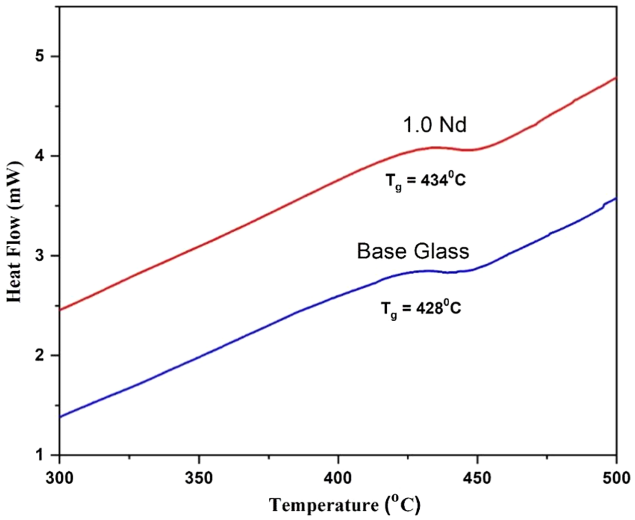

4. Optical Properties

4.1. Absorption spectra

Figure 3 shows the increasing absorption values of $7Bi_2O_3$-$3.3Li_2O$-23SrO-(66.7-x) B_2O_3-xNd_2O_3 where (x = 0.0, 0.1, 0.3, 0.5, & 1.0) doped glasses. The notable absorption bands are caused by $4f^3$–$4f^3$ electronic transitions that occur in the neodymium (III) ions at the $^4I_{9/2}$ ground level to different exciting levels. Nine absorption peaks were observed due to transitions from ground state of $^4I_{9/2}$ of Nd^{3+} to higher energy states. The transition was observed at $^4I_{9/2} \rightarrow {}^4G_{5/2}$ (584 nm) known as hypersensitive since this transition complies with the selection rules of $\Delta L \leq 2$; $\Delta S = 0$ and $\Delta J \leq 2$, $|\Delta S| = 0$; $|\Delta L| \leq 2$ and $|\Delta J| \leq 2$.

4.2. Optical band gap

Optical band gaps have been computed using absorption spectra of the glasses. The band gap relation is evaluated by using the

Figure 3
Absorption spectra of $7Bi_2O_3$-$3.3Li_2O$-23SrO-(66.7-x) B_2O_3-xNd_2O_3 where (x = 0.0, 0.1, 0.3, 0.5, & 1.0) doped glasses

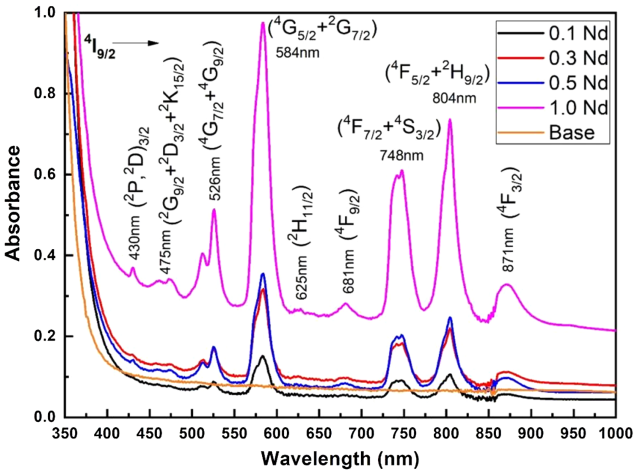

Table 2
Optical bandgap values of $7Bi_2O_3$-$3.3Li_2O$-23SrO-(66.7-x) B_2O_3-xNd_2O_3 where (x = 0.0, 0.1, 0.3, 0.5, & 1.0) doped glasses

Glass sample	Direct bandgap (eV) (±0.01)	Indirect bandgap (eV) (±0.01)	ΔE (eV) (±0.001)	Urbach energy (eV) (±0.001)
0.0Nd	3.335	3.021	0.314	0.178
0.1Nd	3.309	2.928	0.381	0.251
0.3Nd	3.290	2.870	0.420	0.179
0.5Nd	3.229	2.849	0.380	0.249
1.0Nd	3.027	2.823	0.204	0.251

conventional method as reported in Bhogi [11] and Jubu [16]. The indirect bandgap values obtained are 3.021, 2.928, 2.870, 2.849, and 2.823 eV for 0.0, 0.1, 0.3, 0.5, and 1.0 mol% Nd_2O_3 concentrations, respectively. The direct bandgap values obtained are 3.335, 3.309, 3.290, 3.229, and 3.027 eV for 0.0, 0.1, 0.3, 0.5, and 1.0 mol% Nd_2O_3 concentrations, respectively, as shown in Table 2 and displayed in Figure 4 (a–b). Band gap value shows

Figure 4
Tauc's plot for $7Bi_2O_3$-$3.3Li_2O$-23SrO-(66.7-x) B_2O_3-xNd_2O_3 where (x = 0.0, 0.1, 0.3, 0.5, & 1.0) doped glasses. (a) Direct bandgap $(\alpha h\nu)^2$ and (b) indirect bandgap $(\alpha h\nu)^{1/2}$

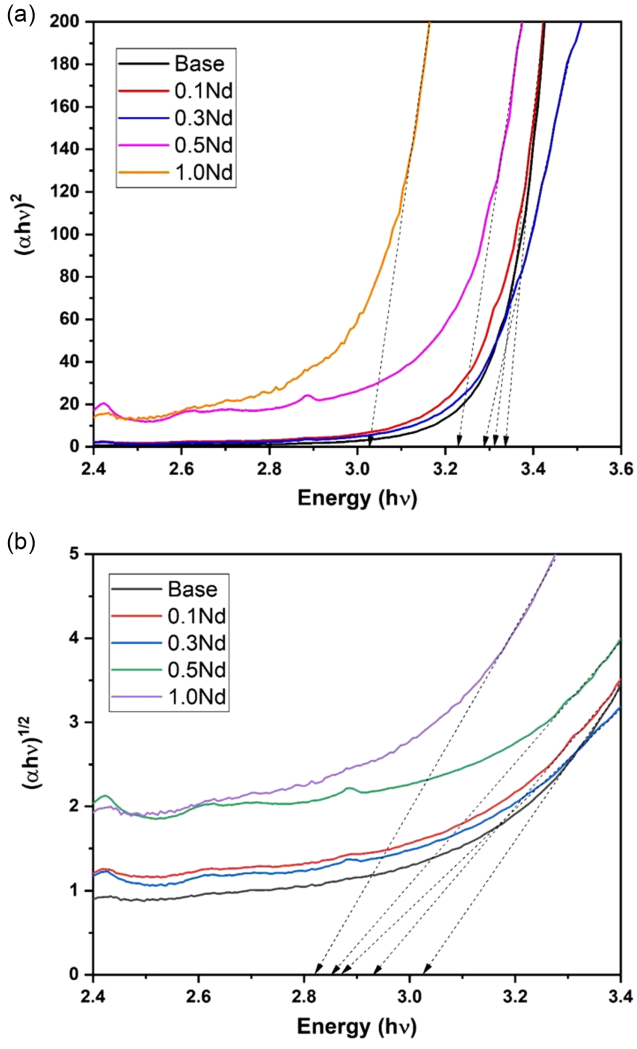

downtrend with addition of Nd_2O_3 concentration due to defect in their bond. The photon energy is effectively explained by three fascinating processes: fundamental absorption, exciton absorption, and valence-band acceptor absorption. In the amorphous states, short-range order also affects the optical absorption. Such defect bond influences the degree of localized states and consequently the increase of donor center in the glass matrix. The decreasing trend of band gap values suggest that the available bridging oxygen (BO) atoms breaks down to convert non-bridging oxygen (NBO) in the network. Urbach energy has been evaluated, and values are found to be 0.178, 0.251, 0.179, 0.249, and 0.251. Urbach energy provides information of non-bridging B-O units in the glass network. Thus, the reduction of band gap is observed with addition of Nd_2O_3 content with increase in Urbach value. The concentration of Nd_2O_3 in the glass causes significant changes in its density and beyond 0.5 mol% they intend to enter the network forming sites thereby showing disorderness in the borate structure. It seems that there may be a correlation between localized electron concentration increases and the transformation of bridging oxygen (BOs) into non-bridging oxygen (NBOs) in addition of Nd_2O_3 content. This change has been observed to result in an increase in polarizability and a reduction in the optical band gap and Urbach energy. Hence, the refractive index of the glass increases with addition of Nd_2O_3 content.

4.3. Judd-Ofelt (JO) analysis

We present the experimental (f_{exp}) and theoretical oscillator strength (f_{cal}) calculations from the absorption spectra, which we have discussed according to expressions as discussed in Monisha [17] and Kotb [1]. Hence, the JO [18, 19] theoretically calculated oscillator strengths (f_{cal}) using Equation (1):

$$f_{cal} = \sum_{\lambda=2,4,6} \Omega_\lambda (\Omega J \| U^\lambda \| \Psi' J')^2, \quad (1)$$

where U^λ is a tensor operator of rank λ, Ωλ (λ = 2, 4, 6) is the JO intensity parameter, and $T = \frac{8\pi mc\upsilon^2}{3h(2J+1)} \frac{(n^2+2)^2}{9n} e^2$ is a constant where v is the wavenumber of each absorption band, h is the Planck's constant, n is the glass sample's refractive index, J is the total angular momentum, and m and e are, respectively, the mass and charge of an electron.

Carnall [20] compared a computed expression presented by Judd as the same as the experimentally discovered band intensities in the Ln3+ solution absorption spectra.

$$f_{exp} = C \int \alpha\ (\upsilon) d\upsilon = 4.318\ \times \int \alpha(\upsilon) d\upsilon, \quad (2)$$

where $C = \frac{2.303\ mc^2}{\pi e^2 N} = 4.318$ is a constant.

$\alpha(\upsilon)$ is the molar extinction coefficient at wavenumber ν (cm^{-1}) of every absorption band, where N is Avogadro's number. The JO parameters are found by taking the least square fit from the f_{exp} and f_{cal}, respectively, from Equations (1) and (2). Equation (3) provides an expression for the fitting values in terms of the magnitude of the root mean square (*rms*).

$$\delta rms = \sqrt{\frac{\sum_{i=1}^{N} (f_{exp} - f_{cal})^2}{N}}, \quad (3)$$

where N shows the number of levels.

The f_{exp} and f_{cal} of the absorption levels are shown in Table 2. Using Equation (2), the f_{exp} of each absorption band was calculated. The values of the matrix element $\|U^\lambda\|$ in the literature are essentially unaffected by the surrounding environment [21]. Table 2 shows that the values of the oscillator strengths from ground state $^4I_{9/2}$ transition to higher level transitions. This transition is hypersensitive and highly dependent on the Nd^{3+}-surrounding environment. The Ω_2 is helpful in determining the covalency between Ln^{3+} and its neighboring constituent as well as the state of the asymmetric environment surrounding lanthanides ions, while the Ω_4 and Ω_6 offer details on the bulk characteristics of the samples, such as their rigidity and modulus.

We have obtained data on the oscillator intensities for an electric dipole that is created in the Nd^{3+} doped $7Bi_2O_3$-$3.3Li_2O$-23SrO-$66.7B_2O_3$ glasses as listed in Table 3. It is proposed that the δ_{rms} value from Table 3 may be used to estimate the quality of fit. δ_{rms} values are 0.612 0.574, 0.532, and 0.513 for 0.1Nd, 0.3Nd, 0.5Nd, and 1.0Nd glasses, respectively. The δ_{rms} deviation validates the JO theory by confirming that the calculated and experimental oscillator strengths are exactly in line with each other.

4.4. JO parameters

We would like to present the values of the JO intensity parameters Ω_λ ($\lambda = 2, 4, 6$) obtained using the experimental and theoretical oscillator strengths. These values are displayed in Table 3 and presented in Figure 5. The intensity parameters (Ω_2, $_4$, and $_6$) for present glasses are expected to increase as the amount of

Table 3
Judd-Ofelt values of experimental ($f_{expt.} \times 10^{-6}$), theoretical ($f_{cal.} \times 10^{-6}$) oscillator strength, and rms deviations of Nd^{3+} doped $7Bi_2O_3$-$3.3Li_2O$-23SrO-$66.7B_2O_3$ glasses

			0.1 Nd		0.3 Nd		0.5 Nd		1.0 Nd	
Transition from ground state $^4I_{9/2}$ →	λ (nm)	Energy cm^{-1}	f_{exp}	f_{cal}	f_{exp}	f_{cal}	f_{exp}	f_{cal}	f_{exp}	f_{cal}
$^4F_{3/2}$	871	11481	1.201	1.255	1.017	1.552	1.415	1.919	1.441	2.112
$^4F_{5/2} + {}^2H_{9/2}$	804	12437	4.033	4.314	5.274	5.397	6.417	6.379	6.988	6.678
$^4F_{7/2} + {}^4S_{3/2}$	748	13368	4.229	4.772	5.145	5.045	6.142	6.748	6.001	6.076
$^4F_{9/2}$	681	14684	0.297	0.315	0.771	0.598	0.818	0.711	1.084	0.976
$^2H_{11/2}$	625	16000	0.334	0.374	0.199	0.109	0.200	0.174	0.123	0.174
$^4G_{5/2} + {}^2G_{7/2}$	584	17123	6.673	6.871	8.871	8.912	10.011	10.171	16.131	16.244
$^4G_{7/2} + {}^4G_{9/2}$	526	19011	1.381	1.207	3.171	3.247	3.411	2.932	4.102	3.987
$^4G_{9/2}$	475	21052	0.761	0.907	2.378	1.535	2.165	1.197	2.541	1.781
$^2K_{15/2} + {}^2G_{9/2} + ({}^2D, {}^2P)_{3/2}$	430	23255	0.870	0.788	1.241	0.992	1.310	0.904	1.417	0.981
δ_{rms} deviation			0.612		0.574		0.532		0.513	

Figure 5
Judd-Ofelt parameter (Ω_λ) as a function of $7Bi_2O_3$-3.3Li_2O-23SrO-(66.7-x) B_2O_3-xNd_2O_3 where (x = 0.1, 0.3, 0.5, & 1.0) doped glasses

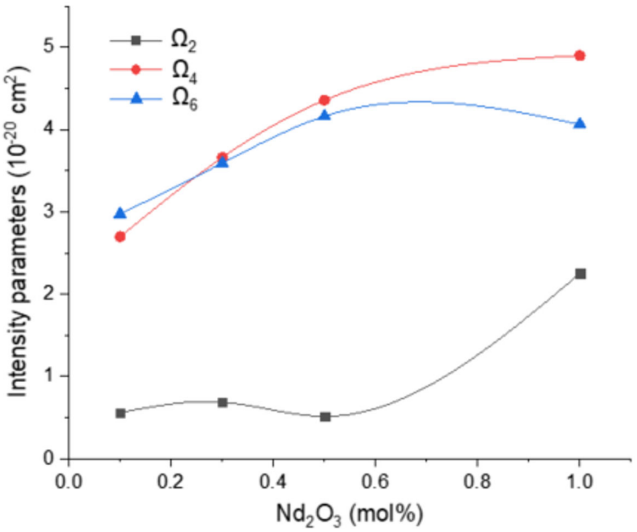

Figure 6
Variation of spectroscopic quality factor (χ) as a function of Nd_2O_3 content

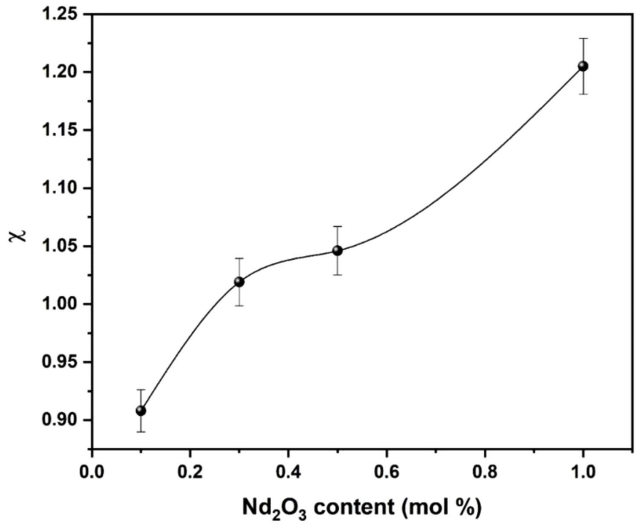

Nd_2O_3 in the host glass increases, according to Figure 5. However, Ω_6 exhibits a slope change at about 0.2 mol% of Nd_2O_3.

It is noted that the Ω_2 parameter is indication of covalent bonding density while Ω_4 and Ω_6 are related to host matrix's rigidity. The dependence of JO parameters on Nd_2O_3 concentration is shown in Table 4. It is our observations that the doped neodymium (III) ions and ligand anions exhibit low covalence and high ionic selectivity and that the neodymium (III) ion surrounding atmosphere is minimal in asymmetry; hence, it is concluded that they do not contribute to the stimulated emission parameter at NIR region [22] and are characteristics of the prepared Nd^{3+} ions doped glass composites. Out of all the JO parameters, the glass samples exhibit Ω_4 high, meaning that bulk properties like stiffness and modulus are high. In contrast to Ω_2, Ω_4 and Ω_6 are typically disregarded due to their high sensitivity to the chemical makeup of their hosts.

It is concluded that $\Omega_6 > \Omega_2 > \Omega_4$ for 0.1Nd glass and $\Omega_4 > \Omega_6 > \Omega_2$ for other samples such trend suggests that the reduction of asymmetric environment around Nd^{3+} ions was observed. It is also interesting to note that 1.0 mol% Nd_2O_3 glass shows Ω_2 lower value than compared with other concentrations suggesting their role in network forming making them more symmetry around rare-earth ions environment. A unique characteristic of the $^4F_{3/2} \rightarrow {}^4I_{11/2}$ transitions of Nd^{3+} emission intensity could be the ratio of Ω_4 to Ω_6, which is referred to as the spectroscopic quality factor ($\chi = \Omega_4/\Omega_6$) [22], its values are listed in Table 4, and its dependence on Nd_2O_3 concentration is displayed in Figure 6. One could argue that the $^4F_{3/2} \rightarrow {}^4I_{11/2}$ laser transition is more intense the smaller the value of χ.

The emission (A_{em}) to excited state absorption (A_{ESA}) intensity ratio was used to calculate the amplification factor as a function of JO parameters. This suggests that amplifying applications are possible, as shown in Table 4. The amplification factor was evaluated using $A_{em}/A_{ESA} = 0.21\Omega_6 \ / \ (0.11\Omega_2 + 0.063\Omega_4)$. As shown in Table 5, the obtained JO and spectroscopic quality factor values are compared with other literature. It is noted that the prepared glasses are well within the limits and comparable with literature. Also, it is noted that the spectroscopic quality factor is higher than compared to other glasses reported.

4.5. Radiative properties and emission spectra

The radiative transition probability (A_T), radiative lifetime (τ_{rad}), branching ratio (β_R), stimulated emission cross-section $\sigma(\lambda_P)$, and effective line width $\Delta\lambda_{eff}$ are, respectively, given in Equations (4–8),

$$A_T(\Psi J) = \sum A(\Psi J, \Psi' J') \tag{4}$$

Table 4
JO parameters (Ω_λ, λ = 2, 4, 6), spectroscopic quality (χ), and amplification factor (A_{em}/A_{ESA}) for $7Bi_2O_3$-3.3Li_2O-23SrO-(66.7-x) B_2O_3-xNd_2O_3 where, (x = 0.1, 0.3, 0.5, & 1.0) doped glasses

Ω_λ ($\times 10^{-20}$ cm^2)	0.1Nd	0.3Nd	0.5Nd	1.0Nd
Ω_2	0.561	0.688	0.515	2.250
Ω_4	2.699	3.661	4.356	4.898
Ω_6	2.972	3.592	4.162	4.062
JO Trend	$\Omega_6 > \Omega_4 > \Omega_2$	$\Omega_4 > \Omega_6 > \Omega_2$	$\Omega_4 > \Omega_6 > \Omega_2$	$\Omega_4 > \Omega_6 > \Omega_2$
$\chi = \Omega_4/\Omega_6$	0.908 ± 0.02	1.019 ± 0.03	1.046 ± 0.03	1.205 ± 0.04
A_{em}/A_{ESA}	2.693	2.462	2.639	1.541

Table 5
Comparison of Judd-Ofelt parameters ($\Omega\lambda$, $\lambda = 2, 4, 6$) with other reported literature

Glass composition	JO trend	χ	Reference
0.1Nd	$\Omega_6 > \Omega_4 > \Omega_2$	0.908	Present Work
0.3Nd	$\Omega_4 > \Omega_6 > \Omega_2$	1.019	Present Work
0.5Nd	$\Omega_4 > \Omega_6 > \Omega_2$	1.046	Present Work
1.0Nd	$\Omega_4 > \Omega_6 > \Omega_2$	1.205	Present Work
BPbSrWNd1.0	$\Omega_2 > \Omega_4 > \Omega_6$	1.055	[1]
2N	$\Omega_6 > \Omega_2 > \Omega_4$	–	[23]
NAYPO-Nd	$\Omega_2 > \Omega_6 > \Omega_4$	0.86	[24]
NAYPOF-Nd	$\Omega_2 > \Omega_6 > \Omega_4$	0.85	[24]
TB1	$\Omega_2 > \Omega_6 > \Omega_4$	–	[25]
Nd-NP-ZnTe	$\Omega_2 > \Omega_4 > \Omega_6$	–	[26]
BaBiTeNd	$\Omega_2 > \Omega_6 > \Omega_2$	0.48	[27]
Y_2O_3-Al_2O_3-B_2O_3	$\Omega_4 > \Omega_6 > \Omega_2$	1.195	[28]
BSGdCaNd0.5	$\Omega_4 > \Omega_2 > \Omega_6$	1.33	[29]
PNbKA	$\Omega_2 > \Omega_4 > \Omega_6$	1.10	[30]

$$\tau_{rad}(\Psi J) = \frac{1}{A_T(\Psi J)} \quad (5)$$

$$\beta_R(\Psi J, \Psi' J') = \frac{A(\Psi J, \Psi' J')}{A_T(\Psi J)} \quad (6)$$

$$\sigma(\lambda_P)(\Psi J, \Psi' J') = \frac{\lambda_P^4}{8\pi c n^2 \Delta\lambda_{eff}} A_R(\Psi J, \Psi' J') \quad (7)$$

$$\Delta\lambda_{eff} = \int \frac{I(\lambda) d\lambda}{I_{max}} \quad (8)$$

where $I(\lambda)$ represents the emission intensities and I_{max} is maximum emission intensity at 'λ'.

The obtained Ω_λ, refractive index, and data from emission spectra were used to calculate the A_{rad}, σ, and β_R for the glass samples, as listed in Tables 6, 7, and 9, by using the Equations (5) to (8). Depending on JO intensity parameters, the radiative transition properties were calculated, such as radiative properties evaluated using JO parameters, and are presented in Table 6. In the present glass, it is expected to observe highest peak intensity at 1.06 μm of NIR region corresponding to $^4F_{3/2} \rightarrow {}^4I_{11/2}$ transition. It is our understanding that the current glasses are suitable for 1.06 μm NIR laser applications, as evidenced by the comparatively higher branching ratio (Table 6) for the $^4F_{3/2} \rightarrow {}^4I_{11/2}$ transition. The radiative lifetime values tend to decrease with

Table 7
$\sigma_{emi}(\times 10^{-19})$ cm^2 of Nd^{3+} doped $7Bi_2O_3$-3.3Li_2O-23SrO-66.7B_2O_3 glasses

Transitions from $^4F_{3/2} \rightarrow$	σ_{emi} ($\times 10^{-19}$) $^4I_{13/2}$	σ_{emi} ($\times 10^{-19}$) $^4I_{11/2}$	σ_{emi} ($\times 10^{-19}$) $^4I_{9/2}$
0.1Nd	6.210	11.93	5.072
0.3Nd	10.95	16.43	9.372
0.5Nd	12.02	20.44	10.21
1.0Nd	12.87	19.45	11.84

Table 8
Assessment of $\sigma_{emi}(\times 10^{-19}$ cm^2) of Nd^{3+} doped with other glasses

Transitions from $^4F_{3/2} \rightarrow$	σ_{emi} ($\times 10^{-19}$) $^4I_{11/2}$	τ_R (μs)	Reference
0.5Nd	20.4	289	Present Work
2N	7.89	139	[23]
NAYPO-Nd	0.37	427	[24]
NAYPOF-Nd	0.36	441	[24]
Glass A	0.209	117	[31]
Glass B	0.239	116	[31]
Glass C	0.300	113	[31]
Glass D	0.274	105	[31]
Glass E	0.217	97.5	[31]
Glass F	0.166	96.9	[31]
BZBNd10	0.76	110	[33]
BSGdCaNd0.5	0.13	342	[29]
15Gd1Nd	2.201	691	[34]
20Gd1Nd	2.245	696	[34]

Table 9
Gain bandwidth and optical gain of Nd^{3+}-doped $7Bi_2O_3$-3.3Li_2O-23SrO-66.7B_2O_3 glasses

$7Bi_2O_3$-3.3Li_2O-23SrO-66.7B_2O_3 glasses	0.1Nd	0.3Nd	0.5Nd	1.0Nd
	$^4I_{11/2}$			
Wavelength (nm)	1069			
Effective bandwidth ($\Delta\lambda_{eff}$, nm)	38.04	57.80	60.02	57.79
Gain bandwidth, cm^2 ($\sigma_{emi} \times \Delta\lambda_{eff}$),$10^{-26}$	4.538	9.499	12.27	11.24
Optical gain, cm^{2}s ($\sigma_{emi} \times \tau_R$), 10^{-22}	3.137	4.321	5.378	5.117

Table 6
Transition probability (A_{rad}), branching ratio (β_R), and radiative lifetime (τ_R) of Nd^{3+} doped $7Bi_2O_3$-3.3Li_2O-23SrO-66.7B_2O_3 glasses

		0.1 Nd		0.3 Nd		0.5 Nd		1.0 Nd	
Transitions from $^4F_{3/2} \rightarrow$	Energy cm^{-1}	A_{rad} s^{-1}	β_R	A_{rad} s^{-1}	β_R	A_{rad} s^{-1}	β_R	A_{rad} s^{-1}	β_R
$^4I_{15/2}$	5545.0	9.69	0.0048	12.36	0.0045	15.44	0.0045	15.81	0.0042
$^4I_{13/2}$	7462.0	195.11	0.0962	248.99	0.0913	310.97	0.0902	318.40	0.0840
$^4I_{11/2}$	9354.0	990.82	0.4884	1301.75	0.4771	1636.66	0.4746	1744.86	0.4605
$^4I_{9/2}$	11235.0	833.23	0.4107	1165.45	0.4271	1485.29	0.4307	1709.97	0.4513
Total A_{rad} (s^{-1})		2028.85		2728.55		3448.37		3789.03	
τ_R (μs)		492		366		289		263	

Figure 7
Emission spectra of $7Bi_2O_3$-$3.3Li_2O$-23SrO-(66.7-x) B_2O_3-xNd_2O_3 where (x = 0.1, 0.3, 0.5, & 1.0) doped glasses

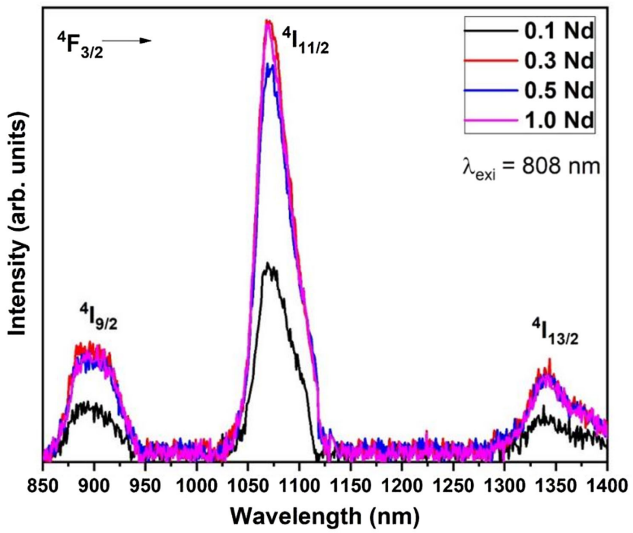

increase in Nd^{3+} ion concentration. Such decreasing trend is due to concentration quenching followed by ET process between Nd^{3+} and Nd^{3+} ions through the cross-relaxation arising from $^4F_{3/2} + {}^4I_{9/2} \rightarrow {}^4I_{15/2} + {}^4I_{15/2}$ transitions [31].

The photoluminescence emission spectra of the glasses excited at 808 nm are displayed in Figure 7. The Nd-doped glass showed three broad emission bands at 890, 1069, and 1340 nm in the near-infrared spectrum at this excitation wavelength. Such three leap energy levels are very important for lasers which can be used in a wide range of scientific, industrial, and telecommunication applications [32]. Our tests have shown that the luminescence intensity decreases due to luminescence concentration quenching above the Nd^{3+} ion concentration of 0.3 mol%. The decrease in NIR fluorescence intensity at higher concentrations, in our case >0.3 mol% Nd^{3+}, is caused by increased ET processes between excited state Nd3+ ions and ground state Nd3+ ions.

The cross-relaxation opens when $^4I_{9/2} \rightarrow {}^4I_{15/2}$ and $^4F_{3/2} \rightarrow {}^4I_{15/2}$ overlaps; hence, the quenching effect is observed [14]. Between the metastable $^4F_{3/2}$ level and its lower $^4I_{15/2}$ level, there is an energy gap of ~5400 cm^{-1}. The emission in NIR region which is located at 1.06 μm of NIR region corresponding to $^4F_{3/2} \rightarrow {}^4I_{11/2}$ transition, while the two other bands at 890 ($^4F_{3/2} \rightarrow {}^4I_{9/2}$) and 1340 nm ($^4F_{3/2} \rightarrow {}^4I_{13/2}$) possess moderate intensities as presented in the partial energy level diagram (Figure 8). For the transition $^4F_{3/2} \rightarrow {}^4I_{11/2}$, stimulated emission cross-section shows higher than the other two transitions. From Table 7, it is evident that stimulated emission cross-section of the present glass shows higher for 0.5Nd glass than other two glasses. σ_{emi} value of 20.44 × 10^{-19} cm^2 and radiative lifetime value of 289 μs for 0.5Nd glass are observed and compared with other reported literature as presented in Table 8. According to the data, glass's values are higher than those of other glasses that have been reported (Table 8). Table 9 displays the figure of merit for laser gain, which is calculated by multiplying the experimental lifetime by the stimulated cross-section. According to Table 9, the current glasses under investigation have a higher figure of merit for laser gain than other glass hosts. It can be concluded that the Nd^{3+}-doped bismuth lithium strontium borate glasses have much better performance in NIR laser device applications.

Figure 8
Partial energy level diagram of $7Bi_2O_3$-$3.3Li_2O$-23SrO-(66.7-x) B_2O_3-xNd_2O_3 where (x = 0.1, 0.3, 0.5, & 1.0) doped glasses

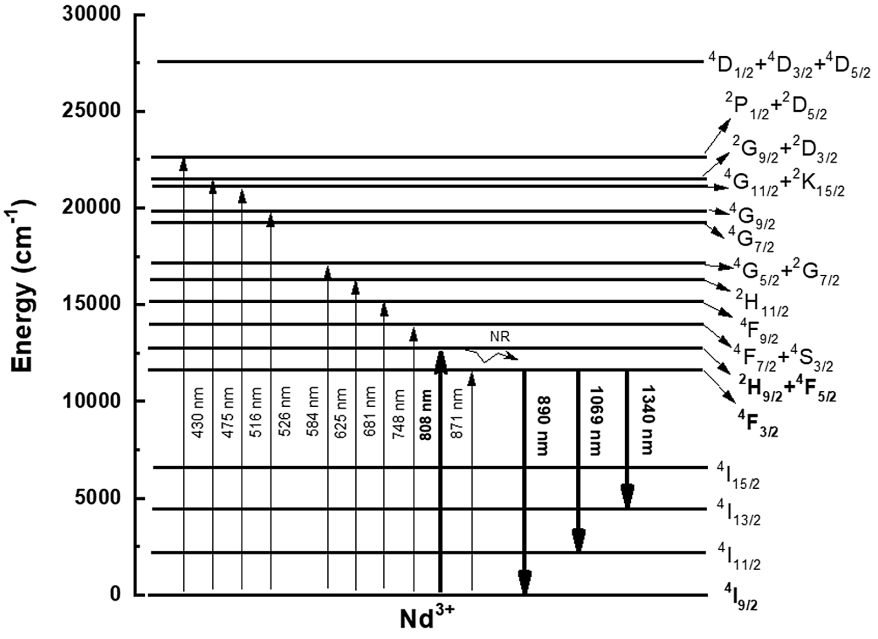

5. Conclusion

In summary, melt quenching was used to create heavy metal oxide-based multicomponent bismuth lithium strontium borate glasses doped with varying concentrations of Nd^{3+} ions. These glasses were then subjected to a series of rigorous tests to analyze their structure, thermal properties, optical characteristics, luminescence, and radiative decay times. Density and refractive index of the prepared glasses were increased with increase in Nd_2O_3 content. Increase in refractive index suggests increase in rigidity of the present glasses which is confirmed with Judd-Ofelt trend $\Omega_6 > \Omega_2 > \Omega_4$ for 0.1Nd glass and $\Omega_4 > \Omega_6 > \Omega_2$ for 0.3Nd, 0.5Nd and 1.0Nd samples. Amplification factor shows >1 suggesting these glasses could be potentially used for amplification. Strong emission peak intensity at 1.06 μm of NIR region corresponds to $^4F_{3/2} \rightarrow {}^4I_{11/2}$ transition. The stimulated emission cross-section value shows a higher value of 20.44×10^{-19} cm^2 and radiative lifetime value of 289 μs for 0.5 mol% Nd_2O_3 glass suggesting their potential role in NIR photonic device applications. The obtained results from stimulated emission cross-section, optical gain, gain bandwidth, and wideband NIR emission of 0.5 mol% of Nd_2O_3-doped glass being a good option for creating O-band optical fiber amplifiers and would suggest that these glasses play a vital role in solid-state NIR emission material applications.

Acknowledgement

Author RRK would like to thank ITMO University for "Implementation of ITMO Fellowship and Professorship Program" St. Petersburg, Russia. The work was carried out in accordance with the Strategic Academic Leadership Program "Priority-2030" for the Siberian Federal University.

Ethical Statement

This study does not contain any studies with human or animal subjects performed by any of the authors.

Conflicts of Interest

The authors declare that they have no conflicts of interest to this work.

Data Availability Statement

Data are available from the corresponding author upon reasonable request.

Author Contribution Statement

R. Rajaramakrishna: Conceptualization, Methodology, Software, Validation, Formal analysis, Investigation, Resources, Data curation, Writing – original draft, Writing – review & editing, Visualization, Project administration. **Evgenia Slyusareva:** Validation, Investigation, Project administration.

References

[1] Kotb, I. E., Okasha, A., Marzouk, S. Y., & Zidan, N. A. (2023). Extensive study on the optical and structural characteristics of Nd3+ doped lead-borate-strontium-tungsten glass system: Judd–Ofelt analysis. *Results in Chemistry*, *5*, 100869.

[2] Issa, S. A., Zakaly, H. M., Badawi, A., Elsaman, R., Tekin, H. O., Showahy, A. A., . . . , & Saddeek, Y. B. (2021). An experimental investigation on structural, mechanical and physical properties of strontium–silicon borate glass system through bismuth-aluminum substitution. *Optical Materials*, *117*, 111124.

[3] Imheidat, M. A., Hamad, M. K., Sayyed, M. I., Alajerami, Y. S. M., Prabhu, N. S., Kamath, S. D., . . . , & Mhareb, M. H. A. (2023). Correlation between mechanical, gamma shielding features and tellurium oxide concentrations in molybdenum aluminum strontium borate glass. *Optik*, *272*, 170336.

[4] Pagoti, R., Panda, S., Patchapureddy, V., Padhi, R. K., Subramanian, B., Jena, H., & Panigrahi, B. S. (2021). Structural and spectroscopic investigations of neodymium-doped strontium borophosphate glass. *Luminescence*, *36*(7), 1706–1715.

[5] Jagannathan, A., Rajaramakrishna, R., Rajashekara, K. M., Gangareddy, J., Pattar, V., Rao, V., . . . , & Kothan, S. (2020). Investigations on nonlinear optical properties of gold nanoparticles doped fluoroborate glasses for optical limiting applications. *Journal of Non-Crystalline Solids*, *538*, 120010.

[6] Morassuti, C. Y., Silva, A. L., Nunes, L. A. O., Lima, S. M., & Andrade, L. H. C. (2023). Effect of radiative loss mechanisms on FIR thermometric parameters of Nd3+-doped lithium tellurite glasses. *Journal of Rare Earths*, *42*(7), 1250–1257.

[7] Zhou, Z., Jiang, X., Leng, Z., Chen, R., Liu, H., Li, C., . . . , & Su, Z. (2023). Research on the near infrared luminescence properties of Nd3+ doped B2O3–BaF2-GeO2/Bi2O3 glass. *Optical Materials*, *141*, 113885.

[8] Koubisy, M. S. I., Afifi, M., Mahmoud, K. A., Tashlykov, O. L., Zatsepin, A. F., Almuqrin, A. H., & Sayyed, M. I. (2022). Synthesis, FTIR, and mechanical as well as radiation shielding characteristics in Nd2O3-doped bismuth lithium borate glasses. *Ceramics International*, *48*(9), 12829–12837.

[9] Madhu, A., Rajaramakrishna, R., James, J. T., Suresh, K., Al-Dossari, M., Abd EL-Gawaad, N. S., & Srinatha, N. (2024). Achieving narrow bandwidth and high stimulated cross-section in Nd3+-doped LiCaB glasses for near infra-red laser amplifiers. *Infrared Physics & Technology*, *136*, 105087.

[10] Patin, M., Nys, K., Wouters, H., Thienpont, H., & Meulebroeck, W. (2022). Using UV-Vis-NIR absorption spectroscopy as a tool for the detection of iron and cobalt in glass: A case-study on HLLA material from the low countries. *Journal of Archaeological Science: Reports*, *44*, 103517.

[11] Bhogi, A., Srinivas, B., Shareefuddin, M., & Kistaiah, P. (2023). Band gap determination by Tauc's, ASF and DASF methods of alkaline earth modified lithium borate glasses co-doped with transition metal ions. *Materials Today: Proceedings*, *92*, 727–731.

[12] Bünzli, J. C. G., & Eliseeva, S. V. (2011). Basics of lanthanide photophysics. In P. Hänninen & H. Härmä (Eds.), *Lanthanide luminescence: Photophysical, analytical and biological aspects* (pp. 1–45). Germany: Springer.

[13] Milewska, K., Maciejewski, M., Žitňan, M., Velázquez, J. J., Galusek, D., Sadowski, W., & Kościelska, B. (2024). Tunable emission and energy transfer of B2O3–Bi2O3–AlF3 glass system doped with Eu3+/Dy3+. *Journal of Luminescence*, *269*, 120440.

[14] Lakshminarayana, G., Kaky, K. M., Baki, S. O., Lira, A., Meza-Rocha, A. N., Falcony, C., . . . , & Mahdi, M. A. (2018). Nd3+-doped heavy metal oxide based multicomponent borate glasses for 1.06 μm solid-state

NIR laser and O-band optical amplification applications. *Optical Materials*, *78*, 142–159.

[15] Pandarinath, M. A., Upender, G., Rao, K. N., & Babu, D. S. (2016). Thermal, optical and spectroscopic studies of boro-tellurite glass system containing ZnO. *Journal of Non-Crystalline Solids*, *433*, 60–67.

[16] Jubu, P. R., Danladi, E., Ndeze, U. I., Adedokun, O., Landi Jr. S., Haider, A. J., . . . , & Yam, F. K. (2024). Comment about the use of unconventional Tauc plots for bandgap energy determination of semiconductors using UV–Vis spectroscopy. *Results in Optics*, *14*, 100606.

[17] Monisha, M., Murari, M. S., Sayyed, M. I., Naregundi, K., Al-Harbi, N., & Kamath, S. D. (2023). Judd-Ofelt analysis and luminescence characteristics of Eu3+ doped Nepheline (NaAlSiO4)-based glass ceramics for solid-state lighting applications. *Journal of Non-Crystalline Solids*, *599*, 121971.

[18] Judd, B. R. (1962). Optical absorption intensities of rare-earthions. *Physical Review*, *127*(3), 750–761.

[19] Ofelt, G. S. (1962). Intensities of crystal spectra of rare-earth ions. *The Journal of Chemical Physics*, *37*(3), 511–520.

[20] Carnall, W. T. (1979). The absorption and fluorescence spectra of rare earth ions in solution. *Handbook on the Physics and Chemistry of Rare Earths*, *3*, 171–208.

[21] Jayasankar, C. K., & Rukmini, E. (1997). Optical properties of Sm3+ ions in zinc and alkali zinc borosulphate glasses. *Optical Materials*, *8*(3), 193–205.

[22] Pal, I., Agarwal, A., Sanghi, S., Aggarwal, M. P., & Bhardwaj, S. (2014). Fluorescence and radiative properties of Nd3+ ions doped zinc bismuth silicate glasses. *Journal of Alloys and Compounds*, *587*, 332–338.

[23] Marzouk, M. A., ElBatal, F. H., Hamdy, Y. M., & ElBatal, H. A. (2023). Judd–Ofelt and photoluminescence analysis of Nd2O3-doped within host fluoroborate glass from the system B2O3–NaF–La2O3. *Applied Physics A*, *129*(7), 505.

[24] Liang, H., Lin, X., Ma, N., Tong, J., He, L., Luo, Z., . . . , & Lu, A. (2024). Judd-Ofelt analysis and NIR spectroscopy properties of Nd3+-doped Na2O/NaF-Al2O3-Y2O3-P2O5 glass and transparent glass-ceramics containing NaYP2O7 crystals. *Ceramics International*, *50*(5), 7807–7816.

[25] Boudchicha, N., Iezid, M., Goumeidane, F., Legouera, M., Prasad, P. S., & Rao, P. V. (2023). Judd–Ofelt analysis and spectroscopy study of tellurite glasses doped with rare-earth (Nd3+, Sm3+, Dy3+, and Er3+). *Materials*, *16*(21), 6832.

[26] Azlan, M. N., Azlina, Y., Shaari, H. R., Hisam, R., Al-Hada, N. M., Umar, S. A., & Kenzhaliyev, B. K. (2024). Judd-Ofelt analysis of zinc tellurite glass doped with neodymium nanoparticles. In *AIP Conference Proceedings, 2750*(1), 080006.

[27] Kumar, J. S., Pavani, K., Gavinho, S. R., Seshadri, M., Anjos, V., Bell, M. J. V., Freire, F. N., . . . , & Graça, M. P. F. (2018). Temperature dependent upconversion and spectroscopic properties of Nd3+ doped barium bismuth tellurite glasses. *Journal of Non-Crystalline Solids*, *498*, 89–94.

[28] Santos, C. N., Mohr, D., Silva, W. F., de Camargo, A. S. S., Eckert, H., Li, M. S., . . . , & Jacinto, C. (2009). Luminescent and thermo-optical properties of Nd3+-doped yttrium aluminoborate laser glasses. *Journal of Applied Physics*, *106*(2), 023512.

[29] Kesavulu, C. R., Kim, H. J., Lee, S. W., Kaewkhao, J., Wantana, N., Kaewnuam, E., . . . , & Kaewjaeng, S. (2017). Spectroscopic investigations of Nd3+ doped gadolinium calcium silica borate glasses for the NIR emission at 1059 nm. *Journal of Alloys and Compounds*, *695*, 590–598.

[30] Manasa, P., Srihari, T., Basavapoornima, C., Joshi, A. S., & Jayasankar, C. K. (2019). Spectroscopic investigations of Nd3+ ions in niobium phosphate glasses for laser applications. *Journal of Luminescence*, *211,* 233–242.

[31] Deopa, N., Rao, A. S., Gupta, M., & Prakash, G. V. (2018). Spectroscopic investigations of Nd3+ doped lithium lead alumino borate glasses for 1.06 μm laser applications. *Optical Materials*, *75*, 127–134.

[32] Lin, X., Liang, H., Jiang, X., Liu, L., Wang, Z., Luo, Y., . . . , & Lu, A. (2022). Thermal and fluorescence properties of Nd2O3-doped Gd2O3-Ga2O3-GeO2 glass based on the Judd-Ofelt theory. *Journal of Non-Crystalline Solids*, *594*, 121810.

[33] Rasool, S. N., Shabeena, S., Kesavulu, C. R., Sekhar, E. C., & Babu, S. (2022). Development of neodymium (III) ions doped sodium fluoro-borate glass composite materials and study of the laser emission. *Optik*, *255*, 168700.

[34] Ramakrishna, R. R., Kothan, S., & Kaewkhao, J. (2023). "GLASS" a novel framework platform for Judd-Ofelt theory: Near infra-red photoluminescence studies of neodymium ions doped in barium zinc gadolinium borate glasses for lasing device applications. *Journal of Materials Science: Materials in Electronics*, *34*(8), 745.

How to Cite: Rajaramakrishna, R., & Slyusareva, E. (2024). Spectroscopy Study of Bismuth Lithium Strontium Borate Glasses Doped with Nd^{3+} Ions for 1.06 μm NIR-Emitting Glasses. *Journal of Optics and Photonics Research*. https://doi.org/10.47852/bonviewJOPR42023085